analytical chemistry

pubs.acs.org/ac Article

Advanced Strategies for Proton-Transfer Reactions Coupled with Parallel Ion Parking on a 21 T FT-ICR MS for Intact Protein Analysis

Chad R. Weisbrod,* Lissa C. Anderson, Christopher L. Hendrickson, Leah V. Schaffer, Michael R. Shortreed, Lloyd M. Smith, Jeffrey Shabanowitz, and Donald F. Hunt

Cite This: *Anal. Chem.* 2021, 93, 9119−9128 Read Online

ACCESS | Metrics & More | Article Recommendations | Supporting Information

ABSTRACT: Proton-transfer reactions (PTRs) have emerged as a powerful tool for the study of intact proteins. When coupled with *m*/*z*-selective kinetic excitation, such as parallel ion parking (PIP), one can exert exquisite control over rates of reaction with a high degree of specificity. This allows one to "concentrate", in the gas phase, nearly all the signals from an intact protein charge state envelope into a single charge state, improving the signal-to-noise ratio (S/N) by 10× or more. While this approach has been previously reported, here we show that implementing these technologies on a 21 T FT-ICR MS provides a tremendous advantage for intact protein analysis. Advanced strategies for performing PTR with PIP were developed to complement this unique instrument, including subjecting all analyte ions entering the mass spectrometer to PTR and PIP. This experiment, which we call "PTR-MS^1-PIP", generates a pseudo-MS^1 spectrum derived from ions that are exposed to the PTR reagent and PIP waveforms but have not undergone any prior true mass filtering or ion isolation. The result is an extremely rapid and significant improvement in the spectral S/N of intact proteins. This permits the observation of many more proteoforms and reduces ion injection periods for subsequent tandem mass spectrometry characterization. Additionally, the product ion parking waveform has been optimized to enhance the PTR rate without compromise to the parking efficiency. We demonstrate that this process, called "rapid park", can improve reaction rates by 5−10× and explore critical factors discovered to influence this process. Finally, we demonstrate how coupling PTR-MS^1 and rapid park provides a 10-fold reduction in ion injection time, improving the rate of tandem MS sequencing.

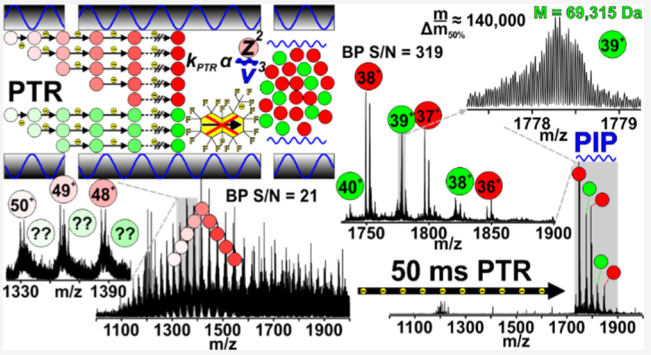

Gas-phase reactions have been reliable analytical tools for mass spectrometrists through the ages.[1−3] These reactions occur ubiquitously during ionization in the source region (APCI,[4] APPI, ESI,[5] etc.) and while ions traverse/reside in the various hardware elements of all mass spectrometry (MS) systems. An example of the latter includes the abstraction of protons by residual water molecules in the vacuum chamber. Often, these reactions are hardly noticeable due to their intrinsically slow rates or they are deliberately minimized to protect instrument performance. However, ion-neutral and ion−ion reactions can be harnessed deliberately within the framework of any mass spectrometer where ions have the proper residence time and are sufficiently mixed to permit reaction, including ion cyclotron resonance (ICR) cells (Penning trap),[6] radio-frequency (RF) multipole storage devices (Paul trap),[7,8] or even beam-type devices.[9] During storage, reagents are introduced to promote the formation of desired gas-phase product ion(s). For example, ion−ion reactions such as electron-transfer dissociation (ETD)[7] or proton-transfer reactions (PTRs)[10] involve reactions with reagent anions to produce charge-reduced product ions. Many pioneers have demonstrated that these reactions provide tremendous analytical value,[11] especially for protein sequencing. This has led to the increased commercial availability of implementations of ion−ion reaction capabilities.[12−14]

Intact or "top-down" protein analysis has been a long-term science driver for the field of analytical MS because it addresses the shortcomings of bottom-up protein analysis.[15] In principle, top-down can provide direct insights into biologically relevant proteoforms[16] including identification via accurate mass and primary amino acid structure determination via tandem MS sequencing. Identification and site localization of post-translational modifications[17] (PTMs) and stoichiometric interrogation of native protein complexes[18] have been demonstrated. Quantification is also achievable on the proteoform level with top-down MS approaches.[19] However,

Received: February 24, 2021
Accepted: June 9, 2021
Published: June 24, 2021

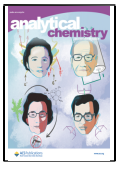

https://doi.org/10.1021/acs.analchem.1c00847
Anal. Chem. 2021, 93, 9119−9128

the analysis of intact proteins is far more challenging than enzymatically produced peptide fragments.[20] Part of the reason for this difficulty is that the ion signal is divided among isotopologues, charge states, proteoforms, adducts, and so forth.[21,22] Division in the ion signal reduces the observed dynamic range and increases the ion accumulation period required for obtaining high-quality tandem MS spectra.

PTR involving multiply charged precursor ions generated by ESI of proteins was first introduced by Stephenson and McLuckey as a means of separating mixtures of overlapping charge-state distributions prior to low-resolution quadrupole ion trap mass analysis.[10,23] While extensive charge reduction can greatly simplify intact and product ion spectra[24−27] of proteins and lessen the requirement for high resolving power, eventually products of PTR are charge-neutralized or fall outside the available m/z range of the mass analyzer. This spurred the development of ion parking[28] and parallel ion parking[29] (PIP) to m/z-selectively halt ion−ion reaction kinetics. PTR coupled with PIP simplifies spectra by concentrating the ion signal into fewer channels, thereby simultaneously increasing signal-to-noise ratio (S/N).

The past 2 decades have seen seismic shifts in the capabilities of Fourier transform mass spectrometry (FTMS) instrumentation that have, in turn, catalyzed advances in top-down proteomics. Robust implementations of PTR, which were commercially released by Thermo Fisher Scientific in 2019, and PIP on today's FTMS instrumentation could overcome many of the challenges associated with top-down proteomics.[19,30] In 2019, Ugrin et al. demonstrated coupling PTR with PIP on a modified Orbitrap Elite for the identification of intact *Escherichia coli* ribosomal proteins.[31] In the same year, Huguet et al. demonstrated the targeted use of PTR for improved detection and intact mass determination of large (>30 kDa) proteins derived from *Pseudomonas aeruginosa*.[14] More recently, Kline et al. utilized PTR to reduce congestion in MS^2 and MS^3 spectra of large intact proteins.[32] These reports illustrate how the appropriate use of gas-phase ion chemistry and careful ion manipulation can dramatically improve intact protein analysis.

Here, we report the implementation of PTR and PIP on a custom 21 T FT ion cyclotron resonance (FT-ICR) MS instrument.[33] In experiments employing multiple activation stages, we show how performing ETD followed by PTR alleviates "extreme" spectral congestion to improve the sequence coverage of a 50 kDa protein (protein A/G) compared to ETD alone. Advanced strategies for PTR coupled with PIP that best exploit the unique instrument configuration of the 21 T FT-ICR MS system are described. This involved the development of pseudo-MS^1 methodology, in which all ions electrosprayed into the mass spectrometer are exposed to the PTR reagent (with no prior isolation; PTR-MS^1) and subjected to PIP. This approach, which we term "PTR-MS^1-PIP", achieves high S/N improvement through the concentration of all observed protein charge and eliminates unnecessary ion-handling/manipulation overhead, saving appreciable analysis time. In proof-of-principle experiments with apomyoglobin, PTR-MS^1-PIP elicited a 10-fold gain in S/N. Single-transient acquisitions yielded an isotopic resolution of protein A/G (50.5 kDa) and an exo-Klenow fragment (68 kDa) in the magnitude mode and exhibited a >10-fold improvement in S/N over the most abundant charge state observed in normal MS^1 acquisitions. In an LC-MS analysis of MCF-7 (*Homo sapiens*) cell lysate proteins, 75% more proteoforms were observed (2472 w/PTR-MS^1-PIP vs 1404 Normal MS^1), along with an increase in the average molecular weight (MW) of the proteins detected, and significant gains in the number of >30 kDa proteoforms were observed.

In efforts to optimize the PIP waveform, we discovered that, under certain conditions, the PTR rate could be accelerated dramatically (~5−10×) over previously reported efforts.[31] This effect, which we refer to as "rapid park", saves valuable analysis time without compromise to parking efficiency. Additionally, the improvement in S/N directly translates to a reduction in the precursor ion injection period for subsequent tandem MS. Ion injection periods represent a significant fraction of the total analysis time. Also, when ion injection periods are long or "maxed out", poor proteoform identification rates result. PTR-MS^1-PIP followed by tandem MS with CID yielded 10× lower ion injection periods for apomyoglobin and equivalent or better sequence coverage across a variety of charge states compared with normal MS^1, followed by CID tandem MS.

EXPERIMENTAL SECTION

Sample Preparation. Pierce Intact Protein Standard Mix and recombinant protein A/G were purchased from Thermo Fisher Scientific (Waltham, MA). Equine myoglobin was purchased from Sigma-Aldrich (St. Louis, MO). These were reconstituted in water and aliquots of myoglobin and protein A/G were diluted to a final concentration of 1 μM in a solution containing 50/50 methanol and 0.1% acetic acid (v/v) for direct infusion. An aliquot of the standard mix was diluted with solvent A (see Liquid Chromatography) to a final concentration of 20 ng/μL for LC-MS.

Pellets of 1×10^7 MCF-7 cells were thawed on ice and suspended in 10 volumes of lysis buffer (4% SDS, 100 mM Tris pH 7.5, 10 mM DTT, 10 mM sodium butyrate, and 1× Thermo Halt Protease and Phosphatase Inhibitor Cocktail). Cell pellets were lysed by heating at 95 °C for 10 min, vortexing every 2 min. Cellular debris was removed by centrifugation at 20,000g for 20 min. Acetone protein precipitation was performed on the supernatant, and the resulting protein pellet was suspended in 150 μL of 1% SDS for quantification via bicinchoninic acid (BCA) assay. Size-based separation of approximately 400 μg of each sample into 12 fractions was performed using a GELFREE 8100 fractionation station with a 10% GELFREE cartridge (Expedeon) following the manufacturer's recommended procedure. Methanol−chloroform precipitation[34] was performed on each fraction to remove SDS, and each pellet was reconstituted in 35 μL of solvent A (0.3% formic acid and 5% acetonitrile in water with % expressed as v/v). Fractions 3 and 4, containing primarily 10−30 kDa proteins, were subjected to LC-tandem MS as outlined below.

Instrumentation. All data presented herein were collected on an in-house-constructed 21 T FT-ICR MS system. This hybrid dual-cell linear RF ion trap 21 T FT-ICR MS system has been previously described.[33] The linear RF ion trap is a modified form of a Velos Pro[35] (Thermo Fisher Scientific, San Jose, CA). The Velos Pro is equipped with a commercial Orbitrap Fusion[36] API inlet/front-end ETD (FETD) reagent ion source (Thermo Fisher Scientific). The glow discharge FETD source enables the simultaneous generation of reagent ions for both ETD and PTR ion−ion reactions.[8] An external multipole storage device (MSD),[37] situated between the velos dual linear RF ion trap (ITMS) and the ICR cell (FTMS),

https://doi.org/10.1021/acs.analchem.1c00847
Anal. Chem. 2021, 93, 9119−9128

allows for multiple ion fills to be collected prior to FTMS acquisition. This device contains an axial field for the sequestration of ions from one end of the MSD to the other. Ions are delivered via a controlled ejection process with an auxiliary RF pseudopotential, as described by Kaiser et al.[38]

The FETD source was further modified to introduce perfluoromethyldecalin (PFMD, m/z 512) reagent anions, and the ion trap control language (ITCL) was modified to include the ability to perform PTR, as described by Ugrin et al.[24] Significant additional code development was required to enable both PTR-MS^1 and rapid ion parking. To enable PTR-MS^1, a single stage of PTR activation was added to the scan matrix for both the normal and AGC matrices. All activation parameters necessary for this step were stored temporarily in the MS^n matrix variables responsible for the first stage of MS^n (see Figures S1−S4 for the long-term stability of this operation mode). Rapid ion parking was enabled by developing a new algorithm to build custom auxiliary waveforms directly within the ITCL using existing hardware with physical modification to optics or circuit boards.

Liquid Chromatography. For each injection, 2−4 μL sample aliquots were loaded onto an in-house-fabricated 360 μm o.d. × 150 μm i.d. fused-silica microcapillary trap column packed 2.5 cm with PLRP-S resin (5 μm particle, 1000 Å pore, Agilent Technologies, Palo Alto, CA). The nano-HPLC system (ACQUITY M-Class, Waters, Milford, MA) was operated at 2.5 μL/min for loading/trapping, and the sample was washed with 95% A for 10 min. Separation was achieved on an in-house-fabricated 360 μm o.d. × 75 μm i.d. fused-silica microcapillary analytical column packed with PLRP-S to 17.5 cm length. For intact protein standards, samples were gradient eluted at 0.3 μL/min with a solvent composition of 5−35% B in 5 min, 35−55% B in 30 min, 55−75% B in 5 min, 75% B wash step for 5 min, and a 5% B re-equilibration step in 15 min (60 min total length). For MCF7 cell lysates, the gradient utilized a solvent composition of 5−15% B in 5 min, 15−55% B in 80 min, 55−75% B in 5 min, and a 5% B re-equilibration step in 15 min (105 min total length). Following separation, samples were directly ionized by microelectrospray ionization using a 15 μm fused-silica PicoTip (New Objective, Woburn, MA) emitter packed 3 mm with PLRP-S resin. A UWPR nanospray source was utilized for the application of the ionization voltage, fixturing the column, and providing fine adjustment for the ESI emitter (http://proteomicsresource.washington.edu/protocols05/nsisource.php).

Mass Spectrometry. For all experiments, the source voltage was biased at 2.5 kV, and the heated capillary temperature was 325 °C. Spectra were collected in the reduced profile mode (with the exception of protein A/G data which utilized the full profile mode) with the ICR mass analyzer. Direct infusion of myoglobin and protein A/G was performed at 0.5 μL/min with a laser-pulled (Sutter P-2000, Novato, CA) fused-silica capillary emitter tip. Myoglobin and protein A/G spectra were taken as the sum of 10 and 50 transients, respectively.

For LC-MS experiments, the instrument was operated with Xcalibur software (Thermo Fisher Scientific). For standards, 50 ng of total protein was injected, and "normal" (denaturing-ESI) MS^1 spectral acquisition was toggled with PTR-MS^1-PIP spectral acquisition. For MCF7 experiments, 4 μL of each reconstituted fraction (F3 and 4) was injected twice: once to acquire only normal MS^1 spectra and once to acquire only PTR-MS^1-PIP spectra.

All LC-MS spectra were acquired from 600 to 2500 m/z, with 5E5 MS^1 AGC target, and were taken as a single transient for standards and as the sum of four transients for MCF7 samples. Transient durations were 1.524 and 0.762 s (corresponding to 1.2 M and 600k resolving power at m/z 200) for standards and MCF7 samples, respectively. The 21 T FT-ICR system at NHMFL routinely produces results with resolving powers at ∼100% of the Nyquist limit for a transient processed via FFT in the magnitude mode. For PTR-MS^1-PIP experiments, a PIP waveform was applied to the x-rods of the high-pressure cell of the dual linear ion trap during PTR. The waveform included frequency components corresponding to m/z 1750−2750, with a normalized activation amplitude of 0.11. The waveform also included a reagent activation window (centered at m/z 512, 20 Th window), where the amplitude was lowered to 0.02.[31] The Mathieu q of the reagent was set to 0.55. The PTR reagent AGC was 5E5, and the entire precursor ion population (no isolation) was exposed to the reagent for 150 ms.

Data Handling. All data were processed in .raw file format (Thermo Fisher Scientific) in the reduced profile mode (noise baseline subtracted). For standards, results were obtained by the visual inspection of the raw data with Xcalibur Qual Browser software (Thermo Fisher Scientific). Additionally, to determine sequence coverage, spectra were deconvolved with the Qual Browser-embedded Xtract algorithm and fragment ions matched to sequences using ProSight Lite[39] with a product ion mass tolerance of ±10 ppm. All protein A/G fragments were manually validated or assigned.

For MCF7, raw files were m/z-to-mass deconvolved with Thermo Protein Deconvolution 4.0 software (Thermo Fisher Scientific) to obtain a count of observed proteoform masses. Xtract parameters were set as follows: 70% fit factor, minimum S/N 2, 10% remainder threshold, two minimum detected charge states, and the charge range of +5 to +50. A sliding window of 0.5 min and 50% offset was used to deconvolute the retention time range of 0−110 min. Deconvolved masses were further aggregated with Proteoform Suite version 0.3.4 (https://github.com/smith-chem-wisc/ProteoformSuite/releases) utilizing merging mass tolerances of 3 ppm, 1 min retention time tolerance, and allowing for the misassignment of monoisotopic masses by up to two isotopologues.

RESULTS AND DISCUSSION

The development of PTR was well ahead of the technology required to take full advantage analytically. Since then, PTR has been employed to alleviate issues associated with extreme spectral congestion[14,24,40,41] in top-down proteomics by reducing the overlap of isotopic peak clusters. For example, ETD is highly effective for intact protein sequence analysis;[42] however, resultant fragment ions are often clustered around the precursor within a narrow m/z range. Application of an additional stage of activation by PTR (ETD-PTR) serves to distribute ETD-product ions more evenly throughout the useable m/z range of the instrument.[43] Figure 1 shows ETD tandem MS spectra of the $[M + 50H]^{50+}$ charge state of recombinant protein A/G (50.4 kDa) without (Figure 1A) and with an additional PTR activation stage (Figure 1B). These spectra were generated from the same number of precursor ions (5E6 cumulative ion target). The insets illustrate the qualitative difference in spectral complexity over a 100 m/z domain. Manually validated fragments matched to the sequence with ProSight Lite following automated spectral

https://doi.org/10.1021/acs.analchem.1c00847
Anal. Chem. 2021, 93, 9119−9128

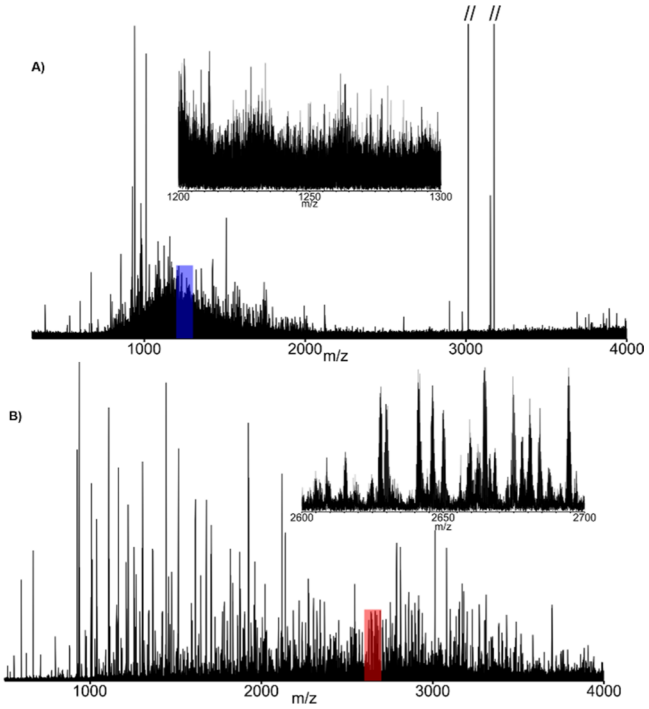

Figure 1. Tandem MS spectra of protein AG $[M + 50H]^{50+}$ (m/z 1010.2) utilizing both ETD alone (A) and ETD followed by a PTR (B). These results illustrate the importance of relieving "spectral congestion", even with ultrahigh-resolution FT-ICR MS (see Figure S1 for identified fragment ion maps).

deconvolution with the Xtract algorithm yielded 12% sequence coverage with ETD-only versus 39% from the ETD-PTR spectrum (see Figure S5 for fragment ion maps). Additionally, PTR provides dramatic S/N improvements that originate from the dependence of the rate of charge reduction on the precursor charge state. Higher-charged fragments are preferentially charge-reduced, and fragment ion current is collapsed into fewer individual charge states as the reaction progresses. This also simplifies the resulting mass spectrum for a more straightforward data interpretation (either manually or algorithmically).

By pairing PTR with parallel ion parking (PTR-PIP), ion signal that is normally dispersed across a wide m/z domain in the form of a protein charge envelope can be concentrated into nearly a single protein charge state. Implementation of PTR-PIP for intact mass analysis, as described by Ugrin et al.,[31] employed wide (400 Th) linear IT precursor isolation prior to PTR-PIP. While this approach is quite successful, precursor isolation limits S/N improvement, as well as the ability to quantitatively interrogate PTR-PIP data, as more charge states of some protein precursors may be isolated and subjected to PTR-PIP than others. Additionally, ion isolation prior to PTR-PIP requires valuable analysis time. The overhead associated with the unnecessary steps is magnified when multiple fills are performed prior to mass analysis to build ion population, improve S/N, or compensate for reduced ITMS space charge capacity. Executing the steps required to accumulate and isolate these large m/z regions requires ~30−50 ms, but this time must be multiplied by the number of ion fills employed to minimize ITMS space charge effects and improve S/N. This can result in hundreds of milliseconds worth of unnecessary overhead per spectrum. Here, we demonstrate an approach called PTR-MS^1 in which all ions entering the mass spectrometer are exposed to the PTR reagent without any pre-processing/manipulation. The resulting spectrum can be thought of as a "pseudo-MS^1" spectrum. While this approach is entirely decoupled from the application of PIP, it is most effective when PTR-MS^1 is coupled with PIP (PTR-MS^1-PIP). In Figure 2, an example is given where normal MS^1 and PTR-MS^1-PIP conditions are used to analyze an intact protein standard mixture by LC-MS. The spectra were acquired during the apex of the elution from each of two high-MW recombinant proteins: protein A/G (50 kDa) and exo-Klenow fragment (68 kDa). Base peak S/N was improved by a factor of ~13× for protein A/G and by ~18× for the exo-Klenow fragment. Insets within each mass spectrum provide an enhanced view of each isotopically resolved envelope used to calculate S/N. These data are the result of single transient acquisitions in the magnitude mode which represents a significant milestone in FTMS technology. While high MW isotopic resolution has been achieved with both ICR and Orbitrap technology, extensive transient averaging is required on the order of 100's to 1000's of summed transients to achieve a similar result. The S/N improvement imparted by PTR-MS^1-PIP, including the ability to isotopically resolve high-MW proteins in single transients, provides a major benefit to LC-MS analysis of intact proteins.

PTR-MS^1-PIP technology was used to analyze the proteins recovered from *H. sapiens* MCF7 (breast cancer) cell lysate, prefractionated by GELFREE.[44] Due to sample availability limitations, our analysis focused on fractions 3 and 4. We often observed many more proteoforms of a given protein from these samples using PTR-MS^1-PIP (by sometimes 3× or more) compared to normal MS^1. Figure 3 presents one such example in which a proteoform family isotopic peak envelope is detected under both normal MS^1 (Figure 3A) and PTR-MS^1-PIP (Figure 3B) conditions. Using the Qual Browser-embedded Xtract algorithm (Figure 3C,D), 5 co-eluting proteoforms were accurately deconvolved from the normal MS^1 spectrum versus 15 co-eluting proteoforms for the PTR-MS^1-PIP spectrum. For the two samples analyzed, the total number of proteoforms detected following automated peak deconvolution and chromatographic clustering[45] improved by >75% (Figure 4) through the use of PTR-MS^1-PIP (1404 vs 2472 proteoforms; normal MS^1 vs PTR-MS^1-PIP). Other important aspects of the analysis that improved through the use of PTR-MS^1-PIP include the average MW of the proteoforms detected (15.6 kDa vs 20.4 kDa; normal MS^1 vs PTR-MS^1-PIP) and the number of proteoforms >30 kDa (2 vs 133; normal MS^1 vs PTR-MS^1-PIP). Thousands of proteoforms were detectable throughout the duration of the analytical gradient, which indicates that the co-elution of proteoforms occurs ubiquitously throughout the HPLC separation. We attribute the improvement in the detected number of proteoforms to reflect performance improvement from PTR-MS^1-PIP, especially for co-eluting the protein species. The next logical step is to interrogate these species using tandem MS for sequence information and PTM localization; however, at the time of these experiments, tandem MS based upon PTR-MS^1-PIP precursor ion acquisitions required further development of instrument control software.

The PIP waveforms utilized thus far in this study mirrored the waveform frequency and amplitude composition utilized by Ugrin et al.,[31] which demonstrated that kinetic excitation of the reagent anion, in addition to desired charge-reduced precursor ions, enabled far more efficient ion parking in the ITMS, albeit

https://doi.org/10.1021/acs.analchem.1c00847
Anal. Chem. 2021, 93, 9119−9128

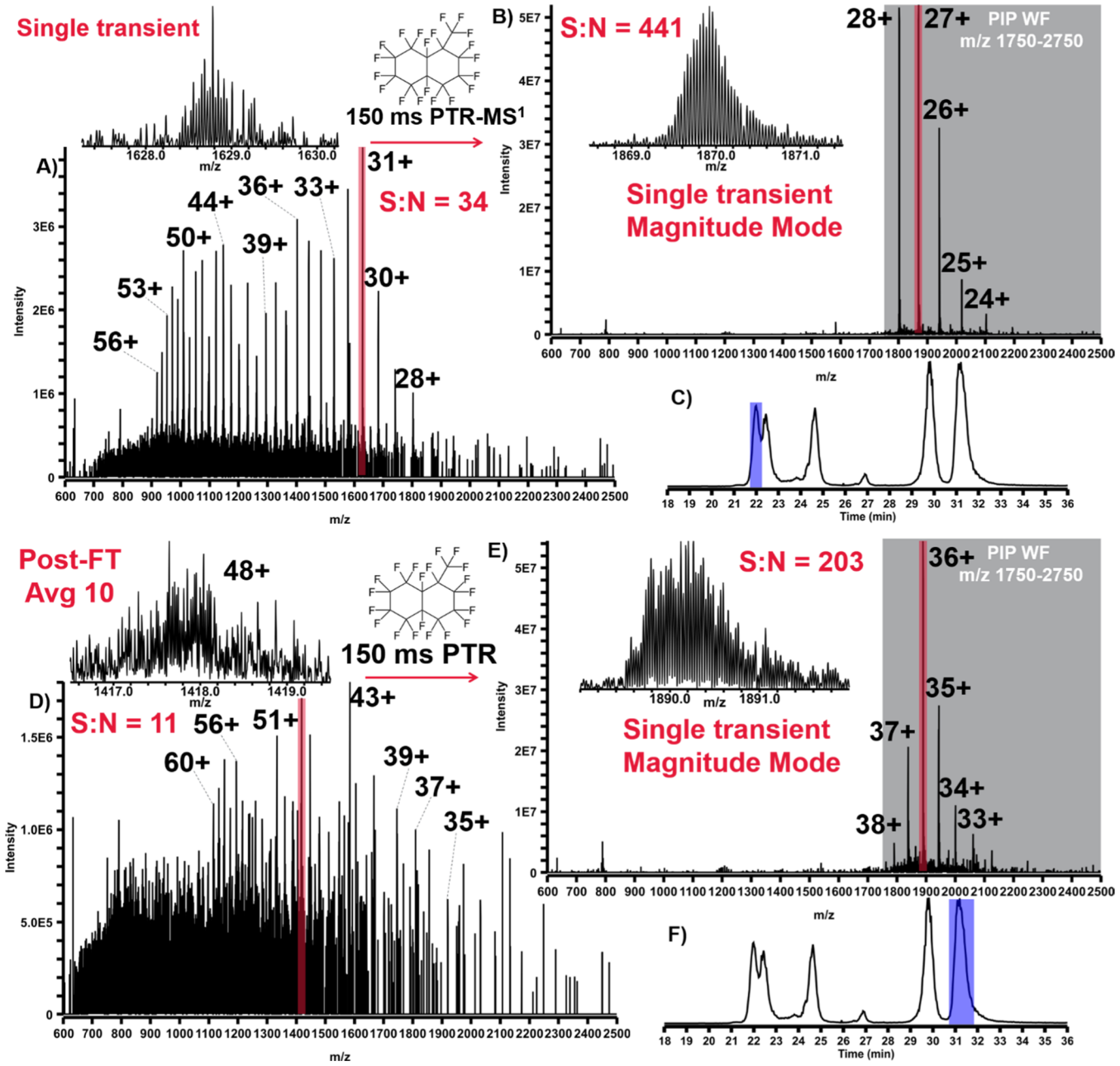

Figure 2. LC-MS analysis of intact protein standard mixture with spectra taken from the apex of elution profiles for both protein AG (50 kDa) and the exo-Klenow fragment (68 kDa). (A) Spectrum of protein AG under normal MS^1 conditions with the most abundant charge state highlighted in red. (B) Spectrum of protein AG under PTR-MS^1-PIP conditions with the most abundant charge state highlighted in red and the range of m/z intended for PIP shaded in gray. (C) LC-MS total-ion chromatogram for the analysis with the region over which protein AG elutes highlighted in blue. (D–F) For the exo-Klenow fragment, the spectra and the LC-MS total-ion chromatogram are the same as that of (A–C).

at a reduced reaction rate. Here, parking efficiency is defined by the following relationship

$$\text{parking efficiency} = \frac{A_{\text{target charge state}}}{A_{\text{all charge states}}} \times 100 \quad (1)$$

where the abundance (A) of the target charge state is divided by the abundance of all observed charge states following PTR-PIP. An unfortunate side effect of PTR is that the precursor charge is consumed through each successive generation of proton transfer. For example, if an $[M + 21H]^{21+}$ precursor was isolated and subjected to PTR-PIP, with the $[M + 14H]^{14+}$ being the desired charge-reduced product, 1/3 of the total charge will be consumed. This presents an upper bound for the yield of the reaction products to be 2/3 the total starting charge (or abundance) prior to PTR. This consumption of charge is unfortunate because the charge capacity of the ion trap cannot be fully exercised, which limits S/N improvement potential when performing PTR-PIP. However, even with this limitation, 10× gain in S/N over normal MS^1 data is often obtainable with our implementation on the 21 T FT-ICR MS at NHMFL (see Figure 2).

Here, under these conditions, high parking efficiency was achieved when computed with eq 1; however, the PTR rate is relatively slow (k = ~50 s^{-1}). With this PIP waveform and reaction rate, measured with apomyoglobin as the analyte, 120

https://doi.org/10.1021/acs.analchem.1c00847
Anal. Chem. 2021, 93, 9119–9128

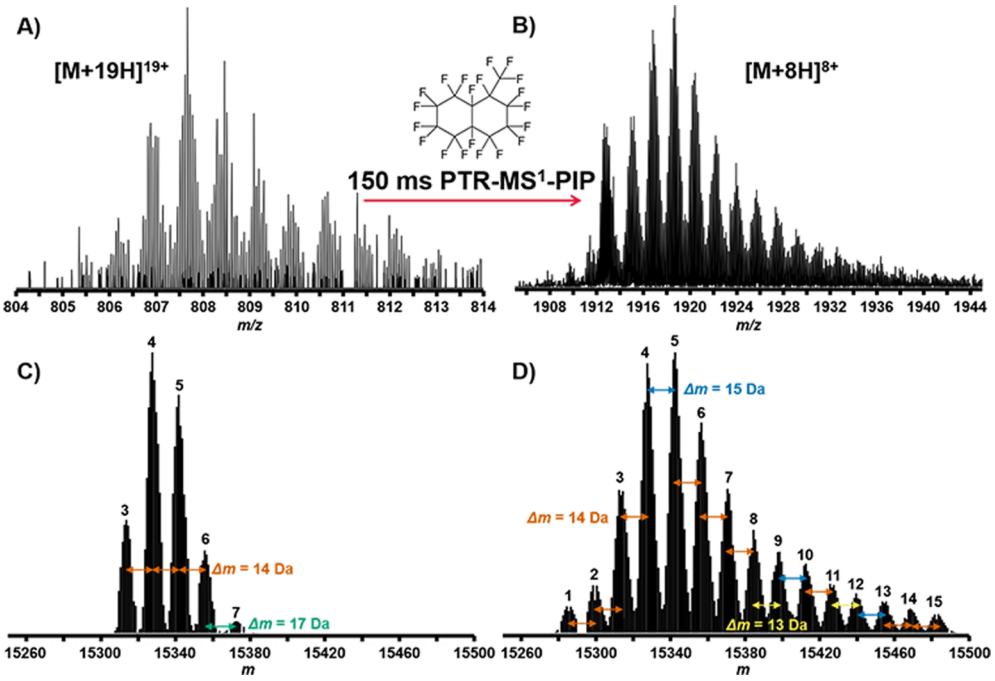

Figure 3. LC-MS analysis of whole cell lysate proteins from *H. Sapiens* MCF7 cells. (A) Region of mass spectrum taken with normal MS^1 conditions containing isotopic peak clusters for a protein exhibiting a "family" of associated proteoforms. (B) The same region measured under PTR-MS^1-PIP conditions shows a more defined set of associated proteoforms from improved S/N. (C) Deconvolution of the peak clusters shown in the normal MS^1 spectrum yielded five proteoforms. (D) Deconvolution of the respective peak clusters of the PTR-MS^1-PIP spectrum yielded 15 proteoforms. Xtract-determined monoisotopic mass differences (Δm, Da) among proteoforms are indicated.

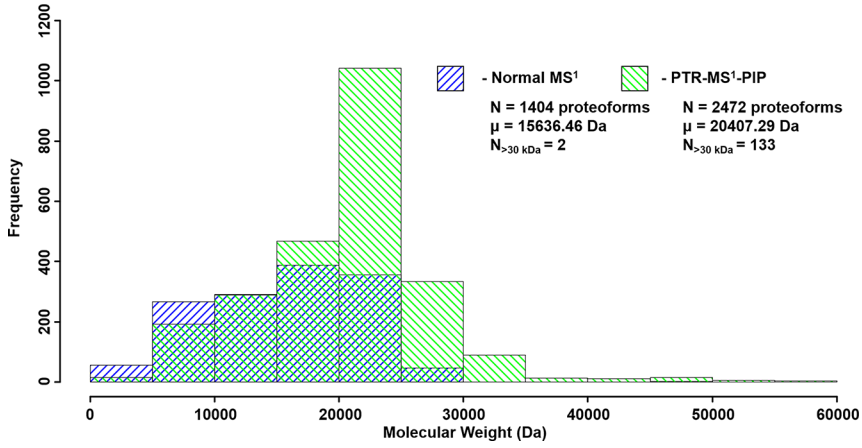

Figure 4. Histogram of MW for all detected proteoforms from the LC-MS analysis of GELFREE fractions 3 and 4 of whole cell lysate proteins derived from *H. sapiens* MCF7 cells. PTR-MS^1-PIP improved the total number of detected proteoforms, especially those of larger MW.

ms is required to convert a purely isolated $[M + 21H]^{21+}$ to the $[M + 14H]^{14+}$ with ~94% parking efficiency (see Figures S6A and S7A). While this experiment was contrived to study reaction rates and to monitor product ion conversion for each successive reaction generation, it represents a lower limit for overall reaction rates possible during PTR-MS^1-PIP type experiments. Taken alone, 120 ms is a relatively short period of time. However, if multiple ion fills are employed to maximize S/N in the FTMS and minimize space charge effects during ion manipulations within the ITMS (including PTR and ETD), the required PTR duration can strain the chromatographic compatibility of the analysis. For example, if 10 ion fills are used with this PIP waveform, 1.2 s duration has been spent simply charge-reducing and parking ions. This represents a significant fraction of total analysis time and fundamentally limits the total number of acquisitions possible per unit time. LC-MS experiments under both targeted or discovery approaches benefit from higher data acquisition repetition rates. Therefore, optimization of the PIP waveform was undertaken to ensure the fastest possible PTR kinetics and highest spectral acquisition rates possible when PTR-MS^1-PIP is utilized at 21 T.

During experiments in which the amplitude of the frequency components responsible for parking the reagent ion and apomyoglobin product ions were optimized, rapid ion parking was discovered. When keeping the product ion parking amplitude constant while iteratively increasing the amplitude utilized for resonant excitation of the reagent anion, the PTR rate decreased until a local minimum in reaction rate was achieved. This minimum also represents the point at which the

https://doi.org/10.1021/acs.analchem.1c00847
Anal. Chem. 2021, 93, 9119−9128

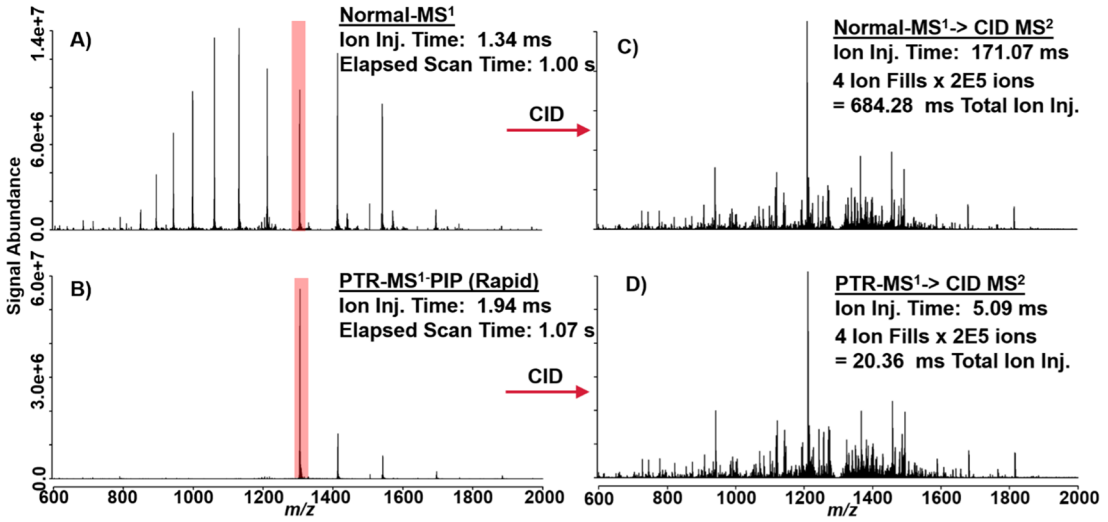

Figure 5. These spectra illustrate proof-of-principle behind the combination of PTR-MS^1, PIP, and rapid ion parking prior to tandem MS analysis. (A) Apomyoglobin mass spectrum under normal MS^1 and (B) PTR-MS^1-PIP with rapid ion parking. $[M + 13H]^{13+}$ is highlighted in red to indicate its isolation and tandem MS by CID. (C) CID spectrum generated from the isolation of $[M + 13H]^{13+}$ under normal MS^1 conditions and (D) PTR-MS^1-PIP with rapid ion parking prior to ion isolation and CID. CID tandem MS spectra are nearly indistinguishable and were generated from the same number of charges (AGC ion target), but precursor ion accumulation times were far lower for the PTR-MS^1-PIP condition.

maximum parking efficiency is achieved and is consistent with observations by Ugrin et al. When the resonant excitation amplitude was increased, collision-activated dissociation of the reagent anion ensues to a small degree, with the predominant reagent fragment ion exhibiting a loss of F (see Figure S8). The radical electron is preserved and the fragment is still a capable PTR reagent. However, the loss of F places this species (m/z 493) outside the frequency range of the PIP waveform for the PTR reagent (20 Th centered at m/z 512), allowing radial excursion of this reactive species to relax back to the thermalized steady state near $r = 0$ over the course of ∼1−2 ms[31] period (see Figure S9). This relaxation in radius and velocity of the reagent anion fragments promotes a concomitant increase in the rate of PTR (see eq 2)

$$k = v\pi\left(\frac{z_1 z_2 e^2}{\mu v^2}\right)^2 \quad (2)$$

McLuckey and Stephenson derived eq 2 to explain dependencies observed during ion−ion reactions, where k is the rate constant, v is the magnitude of the differential velocity between reacting species, z is the integer charge state of the reactants, e is the elementary charge, and μ is the two-bodied reduced mass of the reactants.[46] The rate is inversely proportional to the cube of the differential velocity of the reacting ion clouds. Therefore, when the PFMD reagent anion is activated and undergoes a loss of F, it is no longer being driven by the PIP WF and its effective rate of charge reduction is accelerated relative to the intact reagent anion. Thus, the overall rate constant for the process becomes a linear combination of the k for the original reagent anion and k' for the reagent anion fragment. While the process that leads to rapid ion parking is not yet fully understood, we hypothesize that under the appropriate reagent anion activation conditions, this reactive anion fragment is generated in "just-the-right" abundance to increase the overall PTR rate without excessive charge reduction that would impact parking efficiency (see Figures S6B and S7B). The amplitude of the frequency components used for kinetic excitation of the reagent anion must be carefully controlled to induce this condition (see Figure S10). The onset and rate at which these PTR-active reagent fragment ions are formed from the greater population of reagent anions have been found to be critically important (see Figure S11). When amplitudes are increased further beyond that which induces rapid ion parking, resultant spectra resemble those in which anion excitation was not employed (i.e., parking efficiency is dramatically reduced). Further investigation into the mechanism which enables rapid ion parking is ongoing; however, this initial report is meant to describe this phenomenon and its impact on the performance. Additionally, rapid ion parking was successfully implemented on a second FT-ICR instrument operating at 14.5 T with nearly identical front-end hardware. If rapid ion parking proves to be enabled by progressively altering the reactivity of the reagent anion, it is expected that this process can also be initiated by developing a PIP WF with a time-dependent reagent amplitude component. In this mode, one could modulate the kinetic excitation of the reagent anion slowly, during the PTR period, to maintain the PTR rate and parking efficiency.

In addition to increasing PTR kinetics (see Figure S12) without compromise to parking efficiency, the principal performance impact of rapid ion parking is evident from the following proof-of-principle experiments. In Figure 5A,B, a normal spectrum of apomyoglobin without PTR-MS^1 is shown and can be directly compared against a spectrum in which PTR-MS^1-PIP with rapid ion parking WF was enabled. In this experiment, only 20 ms PTR was required to achieve a 10× boost in S/N (vs 120 ms without rapid ion parking). The total additional time required to conduct PTR-MS^1-PIP with rapid ion parking is 70 ms; this overhead time includes a discrete AGC ITMS acquisition in order to inform the correct number of charges for the subsequent FTMS acquisition (AGC target of 1×10^6 charges). When these ion populations are subject to tandem MS characterization with CID, the primary advantage of rapid ion parking is realized in precursor ion accumulation time. Figure 5A,C shows a single charge state, $[M + 13H]^{13+}$, of apomyoglobin isolated (shown in red) and subjected to CID

https://doi.org/10.1021/acs.analchem.1c00847
Anal. Chem. 2021, 93, 9119−9128

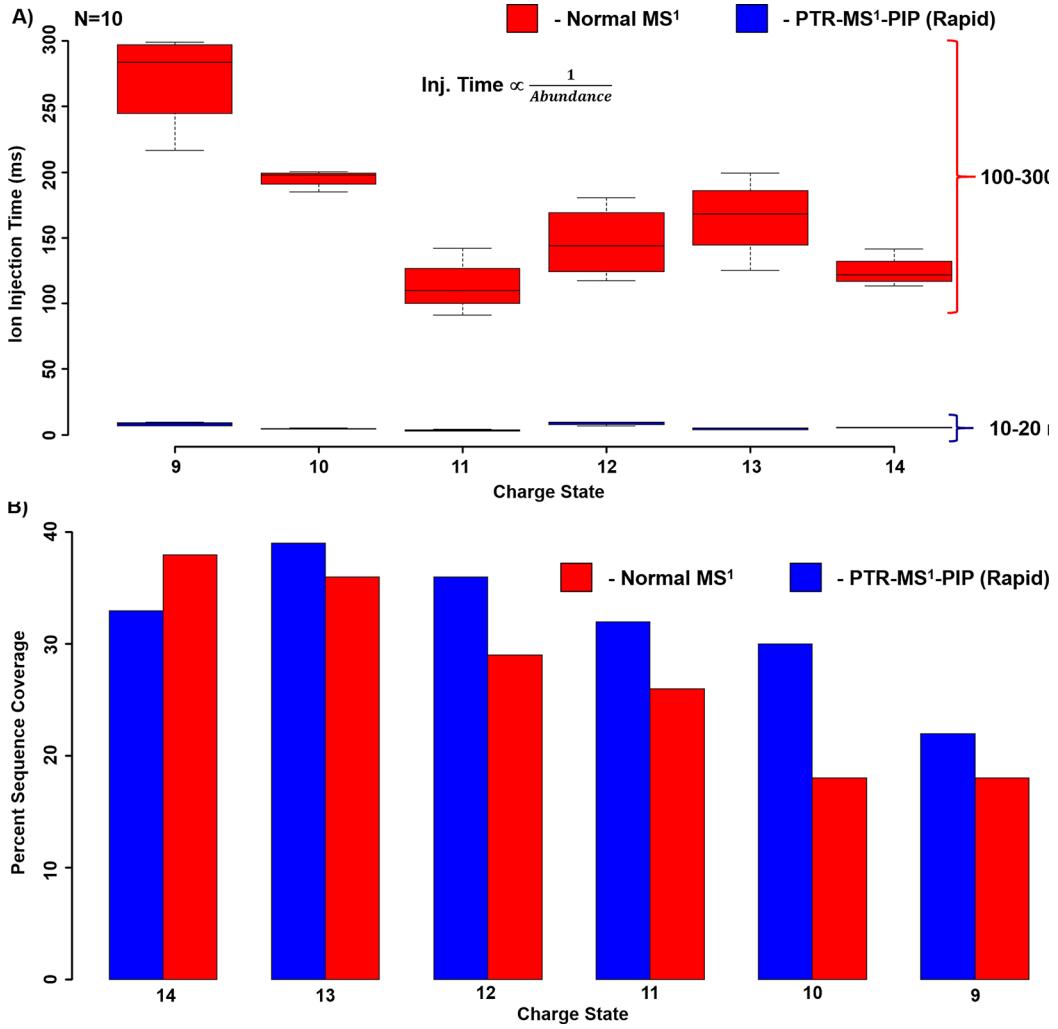

Figure 6. (A) Box and whisker plot of ion injection periods required for tandem MS isolation and fragmentation of various apomyoglobin charge states under normal MS^1 and PTR-MS^1-PIP with rapid ion parking conditions (N = 10). The median injection period is represented by the line through each box, box edges represent the upper and lower quantile, and the whiskers represent the most extreme data points. (B) Bar plot indicating the sequence coverage observed from automated fragment ion assignment using ProSight Lite.

under normal MS^1 conditions. Here, we performed multiple fragment ion fills where each of four fills of the MSD was derived from 2×10^5 precursor charges, requiring 171.07 ms to accumulate per fill (total ion injection time = 684.28 ms). With PTR-MS^1-PIP and rapid ion parking prior to precursor isolation, one can preconcentrate nearly all of the denaturing-ESI charge-state distribution into the desired charge state targeted for tandem MS characterization. In doing so, a dramatic reduction in the ion injection period is observed. In Figure 5B and D, the same charge state ($[M + 13H]^{13+}$) of apomyoglobin has been interrogated by CID tandem MS; however, prior to ion isolation, PTR-MS^1-PIP with rapid ion parking was performed. The ion injection times for the same AGC target used in Figure 5C were decreased by >10× (5.09 ms per ion fill or 20.36 ms total ion injection period). The tandem MS spectra shown in Figure 5C,D have nearly indistinguishable features including S/N and the dynamic range. When these spectra are mined for sequence informative b/y fragment ions with ProSight Lite, nearly identical sequence coverage is obtained (36% Normal MS^1 vs 39% PTR-MS^1-PIP with rapid ion parking).

The reduction in the ion injection period afforded by PTR-MS^1-PIP with rapid ion parking dramatically improves the tandem MS duty cycle. In Figure 6, charge states $14-9^+$ were interrogated with CID tandem MS with and without PTR-MS^1-PIP, and ion injection periods and sequence coverage from the resultant spectra were compared. From these data, a 10-fold reduction in the ion injection period was observed for all charge states (Figure 6A). Sequence coverage for each charge state was similar or better with the PTR-MS^1-PIP rapid ion parking approach, especially for the lower charge states studied (Figure 6B). This is likely the beneficial effect of having converted all the higher charge states of apomyoglobin into the charge state of interest through PTR-MS^1-PIP. We hypothesize that the residual gas-phase structure is retained from their previous charge state or randomized refolding following the loss of charge[47] provides access to a unique set of fragments not attainable through CID of precursors of the same charge states produced by denaturing-ESI alone.

CONCLUSIONS

The pairing of PTR-PIP technology with 21 T FT-ICR MS provides a significant analytical advantage to intact protein analysis. PTR-MS^1-PIP technology provides over 10-fold improvement in S/N compared with conventional precursor

https://doi.org/10.1021/acs.analchem.1c00847
Anal. Chem. 2021, 93, 9119−9128

acquisitions. The greatest benefit is realized with high MW proteins, especially when their signal is spread among a vast number of PTMs and charge states. Many more proteoforms were observed in MCF7 cell analysis compared with conventional precursor ion acquisition. Rapid ion parking improves the PTR rates such that the use of PTR-MS[1]-PIP imparts a negligible overhead in the total acquisition time (~70 ms for apomyoglobin). The observed 10-fold gain in S/N translates to a 10-fold reduction in ion injection periods for apomyoglobin while maintaining tandem MS sequence coverage. These proof-of-principle experiments reveal a promising avenue toward the improvement of both targeted and discovery-based analysis of intact proteins. Further development is required for the incorporation of these approaches into automated data-dependent acquisition workflows. These technological developments will undoubtedly enable a deeper top-down proteome coverage by enabling the detection of lower-abundance proteoforms, and more rapid tandem MS sequencing for greater proteoform identification rates. In principle, PTR-MS[1], PIP, and rapid ion parking could be implemented on existing commercial instruments for a similar performance improvement.

■ ASSOCIATED CONTENT

Supporting Information

The Supporting Information is available free of charge at https://pubs.acs.org/doi/10.1021/acs.analchem.1c00847.

Direct infusion of apomyoglobin subject to PTR-MS[1]; statistical analysis of the base peak; fragment ion maps generated from the tandem MS spectra of protein AG $[M+50H]^{50+}$ under ETD and ETD-PTR conditions; PTR-PIP tandem MS spectra obtained from the isolation of apomyoglobin $[M+21H]^{21+}$; reaction progress plots; high-resolution reagent ion spectra analyzed within FT-ICR; zoomed inset from Figure S8C; plot of the intact reagent anion (PFMD) and the fluorine loss fragment (PFMD-F) as a function of reaction time under various reagent anion parking amplitudes; reaction rate versus reagent parking amplitude; and reaction rate as determined from the precursor ion decay under normal ion parking, rapid ion parking, and uncontrolled PTR (PDF)

■ AUTHOR INFORMATION

Corresponding Author

Chad R. Weisbrod − *Ion Cyclotron Resonance Program, National High Magnetic Field Laboratory, Tallahassee, Florida 32310, United States;* orcid.org/0000-0001-5324-4525; Email: weisbrod@magnet.fsu.edu

Authors

Lissa C. Anderson − *Ion Cyclotron Resonance Program, National High Magnetic Field Laboratory, Tallahassee, Florida 32310, United States;* orcid.org/0000-0001-8633-0251

Christopher L. Hendrickson − *Ion Cyclotron Resonance Program, National High Magnetic Field Laboratory, Tallahassee, Florida 32310, United States*

Leah V. Schaffer − *Department of Chemistry, University of Wisconsin−Madison, Madison, Wisconsin 53706, United States;* orcid.org/0000-0001-6339-9141

Michael R. Shortreed − *Department of Chemistry, University of Wisconsin−Madison, Madison, Wisconsin 53706, United States;* orcid.org/0000-0003-4626-0863

Lloyd M. Smith − *Department of Chemistry, University of Wisconsin−Madison, Madison, Wisconsin 53706, United States*

Jeffrey Shabanowitz − *Department of Chemistry, University of Virginia, Charlottesville, Virginia 22904, United States*

Donald F. Hunt − *Department of Chemistry, University of Virginia, Charlottesville, Virginia 22904, United States*

Complete contact information is available at: https://pubs.acs.org/10.1021/acs.analchem.1c00847

Author Contributions

C.R.W. and L.C.A. contributed equally. The manuscript was written through contributions of all authors. All authors have given approval to the final version of the manuscript.

Notes

The authors declare no competing financial interest.

All raw data and metadata associated with this manuscript can be found at DOI: 10.17605/OSF.IO/TAQN7.

■ ACKNOWLEDGMENTS

The authors thank Thermo Fisher Scientific Research and Development (San Jose, CA) for providing reagent ion source hardware. The Hunt laboratory gratefully acknowledges National Institutes of Health grant GM-037537. The authors also gratefully acknowledge support from the National Science Foundation Division of Chemistry through DMR-1157490 and DMR-1644779 and the State of Florida.

■ REFERENCES

(1) Brodbelt, J. S. *Mass Spectrom. Rev.* **1997**, *16*, 91−110.
(2) Green, M. K.; Lebrilla, C. B. *Mass Spectrom. Rev.* **1997**, *16*, 53−71.
(3) Prentice, B. M.; McLuckey, S. A. *Chem. Commun.* **2013**, *49*, 947−965.
(4) Carroll, D. I.; Dzidic, I.; Stillwell, R. N.; Horning, M. G.; Horning, E. C. *Anal. Chem.* **1974**, *46*, 706−710.
(5) Whitehouse, C. M.; Dreyer, R. N.; Yamashita, M.; Fenn, J. B. *Anal. Chem.* **1985**, *57*, 675−679.
(6) Nibbering, N. M. M. *Acc. Chem. Res.* **1990**, *23*, 279−285.
(7) Syka, J. E. P.; Coon, J. J.; Schroeder, M. J.; Shabanowitz, J.; Hunt, D. F. *Proc. Natl. Acad. Sci. USA* **2004**, *101*, 9528−9533.
(8) Earley, L.; Anderson, L. C.; Bai, D. L.; Mullen, C.; Syka, J. E. P.; English, A. M.; Dunyach, J.-J.; Stafford, G. C.; Shabanowitz, J.; Hunt, D. F.; Compton, P. D. *Anal. Chem.* **2013**, *85*, 8385−8390.
(9) Williams, J. P.; Brown, J. M.; Campuzano, I.; Sadler, P. J. *Chem. Commun.* **2010**, *46*, 5458−5460.
(10) Stephenson, J. L.; McLuckey, S. A. *J. Am. Chem. Soc.* **1996**, *118*, 7390−7397.
(11) Riley, N. M.; Coon, J. J. *Anal. Chem.* **2018**, *90*, 40−64.
(12) McAlister, G. C.; Phanstiel, D.; Good, D. M.; Berggren, W. T.; Coon, J. J. *Anal. Chem.* **2007**, *79*, 3525−3534.
(13) Kaplan, D. A.; Hartmer, R.; Speir, J. P.; Stoermer, C.; Gumerov, D.; Easterling, M. L.; Brekenfeld, A.; Kim, T.; Laukien, F.; Park, M. A. *Rapid Commun. Mass Spectrom.* **2008**, *22*, 271−278.
(14) Huguet, R.; Mullen, C.; Srzentić, K.; Greer, J. B.; Fellers, R. T.; Zabrouskov, V.; Syka, J. E. P.; Kelleher, N. L.; Fornelli, L. *Anal. Chem.* **2019**, *91*, 15732−15739.
(15) Chait, B. T. *Science* **2006**, *314*, 65.
(16) Smith, L. M.; Kelleher, N. L.; The Consortium for Top Down Proteomics. *Nat. Methods* **2013**, *10*, 186−187.
(17) Siuti, N.; Kelleher, N. L. *Nat. Methods* **2007**, *4*, 817−821.

(18) Skinner, O. S.; Haverland, N. A.; Fornelli, L.; Melani, R. D.; Do Vale, L. H. F.; Seckler, H. S.; Doubleday, P. F.; Schachner, L. F.; Srzentić, K.; Kelleher, N. L.; Compton, P. D. *Nat. Chem. Biol.* **2018**, *14*, 36−41.
(19) Schaffer, L. V.; Millikin, R. J.; Miller, R. M.; Anderson, L. C.; Fellers, R. T.; Ge, Y.; Kelleher, N. L.; LeDuc, R. D.; Liu, X.; Payne, S. H.; Sun, L.; Thomas, P. M.; Tucholski, T.; Wang, Z.; Wu, S.; Wu, Z.; Yu, D.; Shortreed, M. R.; Smith, L. M. *Proteomics* **2019**, *19*, 1800361.
(20) Aebersold, R.; Mann, M. *Nature* **2003**, *422*, 198−207.
(21) Riley, N. M.; Mullen, C.; Weisbrod, C. R.; Sharma, S.; Senko, M. W.; Zabrouskov, V.; Westphall, M. S.; Syka, J. E. P.; Coon, J. J. *J. Am. Soc. Mass Spectrom.* **2016**, *27*, 520−531.
(22) Compton, P. D.; Kelleher, N. L.; Gunawardena, J. *J. Proteome Res.* **2018**, *17*, 2727.
(23) Stephenson, J. L.; McLuckey, S. A. *Anal. Chem.* **1996**, *68*, 4026−4032.
(24) Stephenson, J. L.; McLuckey, S. A. *Anal. Chem.* **1998**, *70*, 3533−3544.
(25) Coon, J. J.; Ueberheide, B.; Syka, J. E. P.; Dryhurst, D. D.; Ausio, J.; Shabanowitz, J.; Hunt, D. F. *Proc. Natl. Acad. Sci. USA* **2005**, *102*, 9463−9468.
(26) Holden, D. D.; McGee, W. M.; Brodbelt, J. S. *Anal. Chem.* **2016**, *88*, 1008−1016.
(27) Sanders, J. D.; Mullen, C.; Watts, E.; Holden, D. D.; Syka, J. E. P.; Schwartz, J. C.; Brodbelt, J. S. *Anal. Chem.* **2020**, *92*, 1041−1049.
(28) McLuckey, S. A.; Reid, G. E.; Wells, J. M. *Anal. Chem.* **2002**, *74*, 336−346.
(29) Chrisman, P. A.; Pitteri, S. J.; McLuckey, S. A. *Anal. Chem.* **2006**, *78*, 310−316.
(30) Chen, B.; Brown, K. A.; Lin, Z.; Ge, Y. *Anal. Chem.* **2018**, *90*, 110−127.
(31) Ugrin, S. A.; English, A. M.; Syka, J. E. P.; Bai, D. L.; Anderson, L. C.; Shabanowitz, J.; Hunt, D. F. *J. Am. Soc. Mass Spectrom.* **2019**, *30*, 2163−2173.
(32) Kline, J. T.; Mullen, C.; Durbin, K. R.; Oates, R. N.; Huguet, R.; Syka, J. E. P.; Fornelli, L. *J. Am. Soc. Mass Spectrom.* **2021**, DOI: 10.1021/jasms.1c00062.
(33) Hendrickson, C. L.; Quinn, J. P.; Kaiser, N. K.; Smith, D. F.; Blakney, G. T.; Chen, T.; Marshall, A. G.; Weisbrod, C. R.; Beu, S. C. *J. Am. Soc. Mass Spectrom.* **2015**, *26*, 1626−1632.
(34) Wessel, D.; Flügge, U. I. *Anal. Biochem.* **1984**, *138*, 141−143.
(35) Pekar Second, T.; Blethrow, J. D.; Schwartz, J. C.; Merrihew, G. E.; MacCoss, M. J.; Swaney, D. L.; Russell, J. D.; Coon, J. J.; Zabrouskov, V. *Anal. Chem.* **2009**, *81*, 7757−7765.
(36) Senko, M. W.; Remes, P. M.; Canterbury, J. D.; Mathur, R.; Song, Q.; Eliuk, S. M.; Mullen, C.; Earley, L.; Hardman, M.; Blethrow, J. D.; Bui, H.; Specht, A.; Lange, O.; Denisov, E.; Makarov, A.; Horning, S.; Zabrouskov, V. *Anal. Chem.* **2013**, *85*, 11710−11714.
(37) Wilcox, B. E.; Hendrickson, C. L.; Marshall, A. G. *J. Am. Soc. Mass Spectrom.* **2002**, *13*, 1304−1312.
(38) Kaiser, N. K.; Savory, J. J.; Hendrickson, C. L. *J. Am. Soc. Mass Spectrom.* **2014**, *25*, 943−949.
(39) Fellers, R. T.; Greer, J. B.; Early, B. P.; Yu, X.; LeDuc, R. D.; Kelleher, N. L.; Thomas, P. M. *Proteomics* **2015**, *15*, 1235−1238.
(40) McLuckey, S. A.; Goeringer, D. E. *Anal. Chem.* **1995**, *67*, 2493−2497.
(41) Anderson, L. C.; English, A. M.; Wang, W.-H.; Bai, D. L.; Shabanowitz, J.; Hunt, D. F. *Int. J. Mass Spectrom.* **2015**, *377*, 617−624.
(42) Weisbrod, C. R.; Kaiser, N. K.; Syka, J. E. P.; Early, L.; Mullen, C.; Dunyach, J.-J.; English, A. M.; Anderson, L. C.; Blakney, G. T.; Shabanowitz, J.; Hendrickson, C. L.; Marshall, A. G.; Hunt, D. F. *J. Am. Soc. Mass Spectrom.* **2017**, *28*, 1787−1795.
(43) Anderson, L. C.; Karch, K. R.; Ugrin, S. A.; Coradin, M.; English, A. M.; Sidoli, S.; Shabanowitz, J.; Garcia, B. A.; Hunt, D. F. *Mol. Cell. Proteomics* **2016**, *15*, 975.
(44) Tran, J. C.; Doucette, A. A. *Anal. Chem.* **2008**, *80*, 1568−1573.
(45) Cesnik, A. J.; Shortreed, M. R.; Schaffer, L. V.; Knoener, R. A.; Frey, B. L.; Scalf, M.; Solntsev, S. K.; Dai, Y.; Gasch, A. P.; Smith, L. M. *J. Proteome Res.* **2018**, *17*, 568−578.
(46) McLuckey, S. A.; Stephenson, J. L.; Asano, K. G. *Anal. Chem.* **1998**, *70*, 1198−1202.
(47) Laszlo, K. J.; Munger, E. B.; Bush, M. F. *J. Am. Chem. Soc.* **2016**, *138*, 9581−9588.

https://doi.org/10.1021/acs.analchem.1c00847
Anal. Chem. 2021, 93, 9119−9128